



Effects of different types of guardrails on sand transportation of desert highway pavement

GAO Li¹, CHENG Jianjun^{1*}, WANG Haifeng^{2*}, YUAN Xinxin²

¹ College of Water Resources and Architectural Engineering, Shihezi University, Shihezi 832003, China;

² Xinjiang Institute of Ecology and Geography, Chinese Academy of Sciences, Urumqi 830000, China

Abstract: Guardrail, an important highway traffic safety facility, is mainly used to prevent vehicles from accidentally driving off the road and to ensure driving safety. Desert highway guardrails hinder the movement of wind-blown sand, resulting in the decline of sand transportation by the pavement and the deposition of sand gains on the pavement, and endangering traffic safety. To reveal the influence of guardrails on sand transportation of desert highway pavement, we tested the flow field and sand transport volume distribution around the concrete, W-beam, and cable guardrails under different wind velocities through wind tunnel simulation. Wind velocity attenuation coefficients, sand transportation quantity, and sand transportation efficiency are used to measure sand transportation of highway pavement. The results show that the sand transportation of highway pavement was closely related to the zoning characteristics of flow field and variation of wind velocity around the guardrails. The flow field of the concrete guardrail was divided into deceleration, acceleration, and vortex zones. The interaction between the W-beam guardrail and wind-blown sand was similar to that of lower wind deflector. Behind and under the plates, there were the vortex zone and acceleration zone, respectively. The acceleration zone was conducive to transporting sand on the pavement. The cable guardrail only caused wind velocity variability within the height range of guardrail, and there was no sand deposition on the highway pavement. When the cable, W-beam, and concrete guardrails were used, the total transportation quantities on the highway pavement were 423.53, 415.74, and 136.53 g/min, respectively, and sand transportation efficiencies were 99.31%, 91.25%, and 12.84%, respectively. From the perspective of effective sand transportation on the pavement, the cable guardrail should be preferred as a desert highway guardrail, followed by the W-beam guardrail, and the concrete guardrail is unsuitable. The study results provide theoretical basis for the optimal design of desert highway guardrails and the prevention of wind-blown sand disasters on the highway pavement.

Keywords: desert highway; wind-blown sand; guardrail; sand transportation capacity; wind tunnel test

Citation: GAO Li, CHENG Jianjun, WANG Haifeng, YUAN Xinxin. 2022. Effects of different types of guardrails on sand transportation of desert highway pavement. *Journal of Arid Land*, 14(9): 993–1008. <https://doi.org/10.1007/s40333-022-0030-z>

1 Introduction

Wind-blown sand in desert areas poses a serious threat to agriculture, forestry, and transportation industry. Dry climate, strong winds, and abundant sand sources have made highways and railways across the area prone to wind-blown sand disasters (Dong et al., 2004; Lei et al., 2008; Cheng et al., 2014; Li et al., 2021). Subgrade wind erosion and sand deposition on the highway pavement are caused by the passing wind-blown sand. In severe cases, highways are buried by sand, trains are stopped, and highway traffic is blocked (Han et al., 2003; Xiao et al., 2015; Bruno et al.,

*Corresponding authors: CHENG Jianjun (E-mail: chengdesign@126.com); WANG Haifeng (E-mail: wanghf@ms.xjb.ac.cn)

Received 2022-05-04; revised 2022-08-15; accepted 2022-08-27

© Xinjiang Institute of Ecology and Geography, Chinese Academy of Sciences, Science Press and Springer-Verlag GmbH Germany, part of Springer Nature 2022

2018), which have a serious impact on driving safety. At present, the total length of desert highways built in China exceeds 4000 km, and the total length of desert highways under construction exceeds 1000 km. These desert-crossing highways are the main arteries for highway transportation in China. Therefore, wind-blown sand prevention is still a key engineering and technical problem in road construction and maintenance. Through field investigation, we found that most sand deposition on highways crossing wind-blown sand activity areas is located near the guardrail (Fig. 1), indicating that the guardrail has a great effect on sediment transport and sand transportation of desert highway pavement.



Fig. 1 Sand deposition near the guardrails of desert highways. (a), concrete guardrail; (b), W-beam guardrail (Li et al., 2016); (c), cable guardrail.

To prevent vehicles from accidentally driving off the road due to faults or accidents, people usually installed concrete guardrails (rigid guardrails), W-beam guardrails (semi-rigid guardrails) or cable guardrails (flexible guardrails) on both sides of the highway subgrade, on the median separator, and on bridges to ensure driving safety (Jason et al., 2005; Wang et al., 2011). In desert areas, different forms of guardrails become obstacles in the process of wind-blown sand movement, which disturb the wind-blown sand to varying degrees, reduce the wind velocity, and change the flow field distribution, resulting in reduced sand transportation and sand grain deposition. Sand deposition on highway pavement will lead to the reduction of road surface friction and skid-resistant performance, vehicle slip, obstruction of drivers' sight, and other effects, which endanger driving safety and increase the difficulty and burden of road maintenance work (Pan et al., 2021).

Research on prevention of wind-blown sand disasters along highways and railways has a long history, and the existing measures for prevention and control of wind-blown sand disasters can generally be divided into three categories. The first category includes mechanical sand prevention measures, such as high vertical reed sand barriers, polyethylene (PE)-net sand barriers, sheet-type sand fences, etc. (Cheng et al., 2016a, b; Chen et al., 2019; Cheng et al., 2021), and sand stabilization measures, such as low vertical grass squares, PE grids, sand fixation boards, etc. (Wang et al., 2020; Ding et al., 2021). The second category includes biological sand prevention measures, such as planting sand-fixing plants (*Haloxylon ammodendron* (C. A. Mey.) Bunge, *Tamarix*, etc.) in a certain area on both sides of the highway to build sand blocking and sand stabilization zones (Li et al., 2021), forming natural protective barriers to prevent mobile dunes from invading the highway. The third category includes chemical sand stabilization measures, such as spraying chemical sand stabilization agents on the sand surface to form a consolidation layer for sand fixation (Han et al., 2003). These three measures have been widely used in the prevention of wind-blown sand disasters for roads in desert areas, which play an important role in reducing sand deposition on the road and ensuring the driving safety of vehicles. The above three types of sand prevention measures are all aimed at off-road sand protection systems, and there is little research conducted on the influence of highway structures and accessory facilities on sediment transport. In the practice of sand prevention on desert highway, due to the smooth highway surface, sand disasters along the road can be effectively controlled by making full use of smooth characteristics of the pavement for sand transportation in combination with sand barrier resistance and sand particle stabilization system. Therefore, how to effectively utilize the pavement for sand transportation and related research is very urgent.

Methods such as field observations, wind tunnel tests, and numerical simulation are usually used to study wind-blown sand movement. Among them, wind tunnel testing is a powerful tool to study the aerodynamic characteristics of obstacles and sand transport under artificial simulated atmospheric boundary conditions. Li et al. (2020) conducted scaled-down tests in wind tunnels to simulate the destructive process of sand grains on desert highway by taking sand grains with different diameters and subgrades at different gradients as models. Shi et al. (2021) compared and evaluated the sand prevention performance of two concrete sand-prevention barriers along the railways in strong wind areas using wind tunnel tests and *in situ* monitoring. Wang et al. (2020a, b) preliminarily studied the flow field and sand deposition patterns on both sides of the subgrade and around the median separator of a high-grade highway. Most of studies focused on the characteristics of wind-blown sand fields and sand prevention performance of various sand prevention measures along the highway. Few studies focused on the influence of different types of guardrails on sand transportation of highway pavement using wind tunnel tests.

In this study, based on the urgent need for sand prevention engineering practices for desert highways, wind velocities around the concrete, W-beam, and cable guardrails, as well as pavement sand transportation quantity, were tested by wind tunnel modulation. Wind velocity isoline maps, wind velocity attenuation coefficients, sand transportation efficiency, vertical distribution of sand transportation quantity, and sand transportation characteristics along the desert highway were obtained. Meanwhile, sand transportation of the highway pavement under three types of guardrails was compared. The results might provide a theoretical basis for type selection, structure design, and parameter optimization of desert highway guardrails.

2 Materials and methods

2.1 Materials

The blow-down wind tunnel utilized in this study is mainly comprised of five parts: power section, rectification section, sand supply section, test section, and diffusion section. The whole length was 38 m, the test section length was 21 m, the cross-section size of the test section was 1.3 m (width)×1.0 m (height), and wind velocity was continuously adjustable from 0 to 20 m/s. Previous experiments showed that the wind turbulence degree was about 1.0%, the airflow stability coefficient was less than 1.0%, and the transverse unevenness was less than 2.5%. Wind velocity measuring device included a pitot tube, micro-pressure sensor, and supporting software for wind tunnel system. The axis wind velocity measuring device at the entrance of a test section was the Hot-Wire Anemometer (HWA). The HWA was calibrated with a pitot tube and differential pressure meter before testing. The guardrail height was at the scale of 1:10 according to the Chinese national standard. The height of the concrete guardrail (H_a) was 8.1 cm, the W-beam guardrail (H_b) 7.5 cm, and the cable guardrail (H_c) 11.3 cm. The concrete guardrail was made from poured concrete, the W-beam guardrail consisted of a pillar and waveform iron sheet (the iron sheet height was 3.1 cm), and the cable guardrail was assembled from pillars and steel cables (5 steel cables, each 0.18 cm in diameter). The three types of guardrails were 80 cm in length to avoid the influence of wind tunnel sidewall on the wind field.

2.2 Experimental design

Wind tunnel test was divided into two parts: a flow field test and a sediment transport test. For the convenience of study, an open-field test (with the same wind velocity and sand source, but no guardrail model) was set as a control treatment. When conducting flow field tests in the wind tunnel, wind speeds at different monitoring points were measured using a pitot tube fixed on an adjustable frame, with the monitoring points set at 1.0H, 2.0H, 5.0H, and 10.0H (H is the guardrail height) on the windward side, and 0.0H, 1.0H, 2.0H, 5.0H, 10.0H, 15.0H, and 20.0H on the leeward side of guardrail (Fig. 2). Pitot tube can simultaneously monitor speeds at heights of 1, 2, 3, 5, 7, 10, 15, 30, and 50 cm. After the measured wind velocity data were processed by Surfer software, the wind velocity isoline maps around the three types of guardrails were

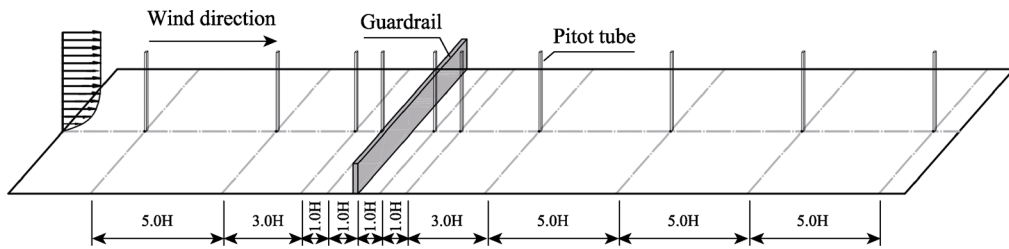


Fig. 2 Layout of the flow field test. H is the height of guardrail.

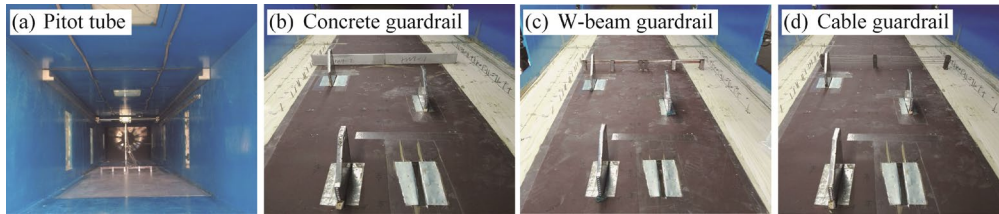


Fig. 3 Flow field and sediment transport measurement. (a), pitot tube; (b), concrete guardrail; (c), W-beam guardrail; (d), cable guardrail.

obtained. The Kriging value was selected as the interpolation.

When sand transport tests in the wind tunnel were conducted, the sand was supplied by means of wind blowing, and the amount of sand source supplied under the same wind velocity and the testing time were consistent. Sandpaper was laid flat on the wind tunnel floor to simulate surface roughness. Sandpaper length ranged from $40.0H$ before the guardrail to $20.0H$ after the guardrail. Installation position of the guardrail remained unchanged. Dune sand collected from the Taklimakan Desert was tiled at the entrance of wind tunnel test section at $100\text{ cm (length)} \times 80\text{ cm (width)} \times 2\text{ cm (height)}$. The device was run at a wind velocity of 8 m/s for 5 min , and photographs were taken to record sand deposition near the guardrail. Pre-testing showed that when a sand sampler was installed outside $2.0H$ on the leeward side of guardrail, the influence of the sand sampler on the sand deposition distribution was avoided, and sand grains of different heights were effectively collected. Therefore, sand sampler was installed at $2.0H$, $5.0H$, $10.0H$, $15.0H$, and $20.0H$ on the leeward side. At the end of the test, sand deposition quantities collected at different heights in the sand collecting box on the leeward side of guardrail were weighed, and sand deposition distributions around the three types of guardrail was observed (Fig. 3). The sand samplers had an overall height of 20 cm , and were distributed vertically and evenly across 20 sand collecting holes, which were $1\text{ cm} \times 1\text{ cm}$. To avoid sand saturation collected by sand samplers due to an excessively long-time test, the test times for 8 , 10 , 12 , and 14 m/s wind velocities in this test were 15 , 7 , 4 , and 3 min , respectively.

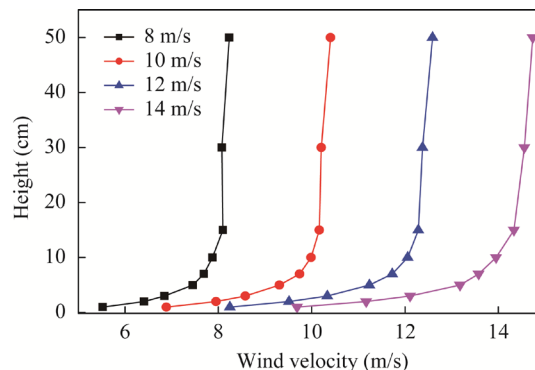


Fig. 4 Wind velocity profiles of the simulated boundary layer

Figure 4 showed wind velocity profiles of the simulated boundary layer measured in the wind tunnel tests, which conformed to a logarithmic distribution. The boundary layer thickness in the test sections was about 15.0 cm, and the maximum height of the guardrail was 11.3 cm, located in the boundary layer. According to the calculation principle of hydrodynamics, the blocking probability of the tunnel section must be less than 5% in wind tunnel simulation, i.e., the percentage of model area to the whole section area must be less than 5% to avoid a deformation effect. In this study, the blocking probabilities of the concrete, W-beam, and cable guardrails were 4.98%, 1.91%, and 0.55%, respectively, and met all requirements. The lowest wind velocity in the test was 8 m/s, and the Reynolds number (Re) was 6.1×10^5 according to the guardrail height. Previous studies have shown that when Re equals or exceeds the minimum independent value of 1×10^5 , the scale model flow would be dynamically similar to that in the full-size case (White, 1996). In the wind tunnel test section, the Froude number (F_r) of grain saltation was 20, which met the minimum F_r criterion proposed by Owen and Gillette (1985):

$$F_r = \text{sqrt}(u_\infty^2 / (gH)), \quad (1)$$

where F_r is the Froude number; u_∞ is the velocity of fluid (m/s); g is the gravitational acceleration (m/s^2); and H is the characteristic length (m).

2.3 Evaluation indicators

At a certain distance from the leeward side and a certain height above the ground, the wind velocity reduction degree is expressed by the wind velocity attenuation coefficient (WVAC) as follows:

$$\xi_{(x,z)} = \frac{v_{0(x,z)} - v_{(x,z)}}{v_{0(x,z)}}, \quad (2)$$

where x is the distance between a test point on the leeward side and the guardrail (H : H is the guardrail height); z is the height of a test point from the ground (m); $v_{0(x,z)}$ is the wind velocity at point (x, z) with no guardrail (m/s); and $v_{(x,z)}$ is the wind velocity at point (x, z) with the guardrail (m/s). The larger the value of WVAC, the more severe the wind velocity attenuation, and the weaker the sand transportation capacity (STC) of the airflow. The area with a larger value of WVAC may become a sand unloading area or sand deposition area.

To reveal the effects of different types of guardrails on sand transportation of desert highway pavement, we used Equation 3 to calculate sand transportation efficiency (STE) of the pavement below $1.0H$ of the guardrail.

$$\eta_x = \frac{\sum_{i=1}^{10} Q_{hxi}}{\sum_{i=1}^{10} Q_{nxi}} \times 100\%, \quad (3)$$

where η_x is the STE of the pavement at distance x (2.0H, 5.0H, 10.0H, 15.0H, and 20.0H) from the guardrail; Q_{nxi} is the sand interception ($\text{g}/(\text{cm}^2 \cdot \text{min})$) of the i^{th} sand collecting box at x with no guardrail arranged; and Q_{hxi} is the sand interception ($\text{g}/(\text{cm}^2 \cdot \text{min})$) of the i^{th} sand collecting box at x with guardrail arranged. The higher the STE, the better the STC, and the less the deposited sand when that type of guardrail is used.

3 Results

3.1 Flow field distribution around the guardrail

The quantity of sand transported on the highway pavement and deposition trends are affected and controlled by the flow field distribution around the guardrail. Figure 5 shows the wind velocity isoline maps of three types of guardrail at a wind velocity of 12 m/s. The positive and negative values represent the leeward and windward sides of guardrail, respectively. It can be seen from

Figure 5 that the flow field around the guardrail changed due to their blocking effects, and the velocity isoline maps for the three types of guardrail also differed significantly. The flow field around the concrete guardrail was divided into three areas: a deceleration zone on the windward side, an upper acceleration zone, and a vortex zone on the leeward side (Fig. 5a). The airflow around the W-beam beam was hindered by the corrugated plate, above and below, which produced a detour flow. When the upper airflow was raised, its speed increased, forming an acceleration zone. The separated upper and lower airflow generated a vortex zone on the leeward side of guardrail. When the reverse airflow met the forward airflow accelerated under the plate, the forward wind velocity decreased, forming a deceleration zone (Fig. 5b). The cable guardrail had little influence on the incoming wind velocity, which caused increased airflow pulsation on the windward side and no clear change in flow field distribution on the leeward side (Fig. 5c).

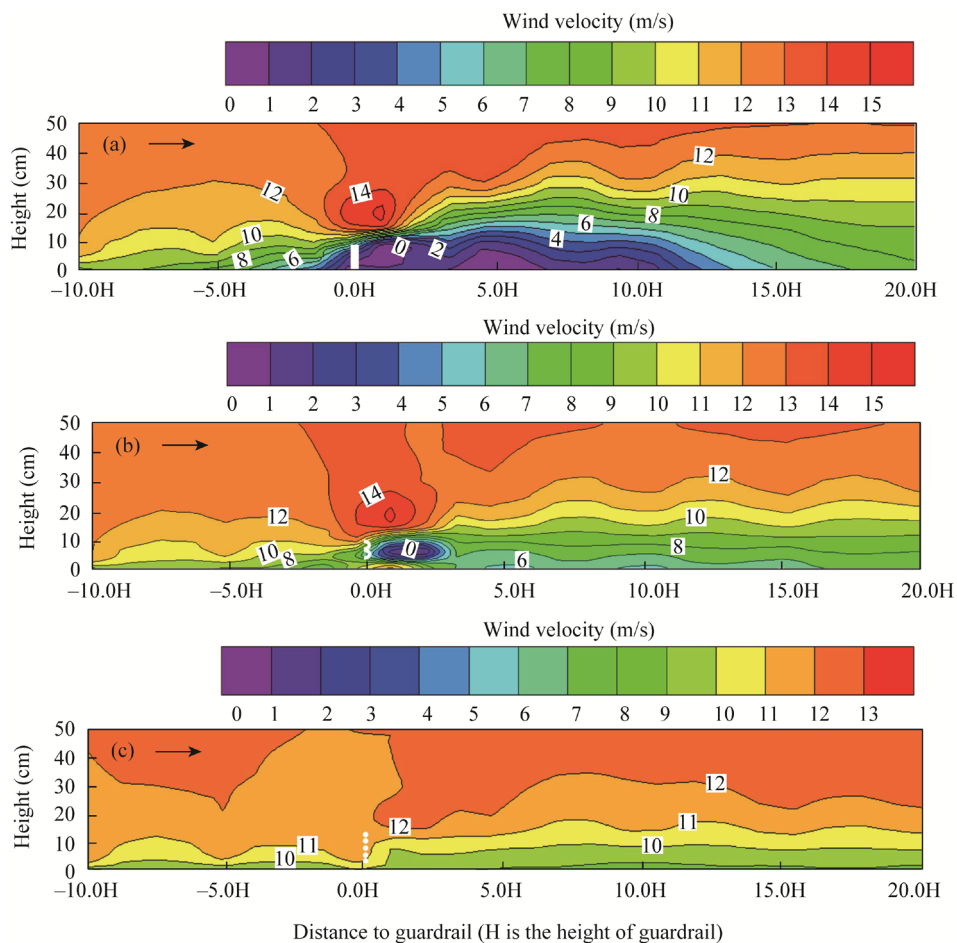


Fig. 5 Isoline maps of wind velocity distribution around different types of guardrail under the velocity of 12 m/s. The positive and negative values represent the leeward and windward sides of guardrail, respectively. (a), concrete guardrail; (b), W-beam guardrail; (c), cable guardrail.

Based on the wind tunnel test results and wind velocity isoline maps, the evolution of streamlines and wind patterns around the three types of guardrail are shown in Figure 6. As the airflow approached the concrete guardrail, the cross section decreases, the normal airflow was blocked, and the velocity in front of the guardrail decreased. When the airflow passed through the concrete guardrail, the cross section increased. Airflow accelerated to lift at the top of the guardrail, forming a reverse flow area on the leeward side due to the influence of the reverse pressure gradient, which caused sand deposition (Fig. 6a). The W-beam guardrail surface was not ventilated, and the area under the guardrail was ventilated, so the velocity and direction of airflow

through the guardrail changed. The top and bottom airflows were separated by squeezing, accelerating airflow formed at the upper and lower ends of the plate, and a small vortex zone formed on the leeward side. After the airflow under different velocities converged again, sand was deposited at a distance behind the guardrail (Fig. 6b). The cable guardrail had good ventilation and hardly hindered airflow, so its streamlines resumed and remained in the inflow state soon after it was slightly offset near the cable (Fig. 6c).

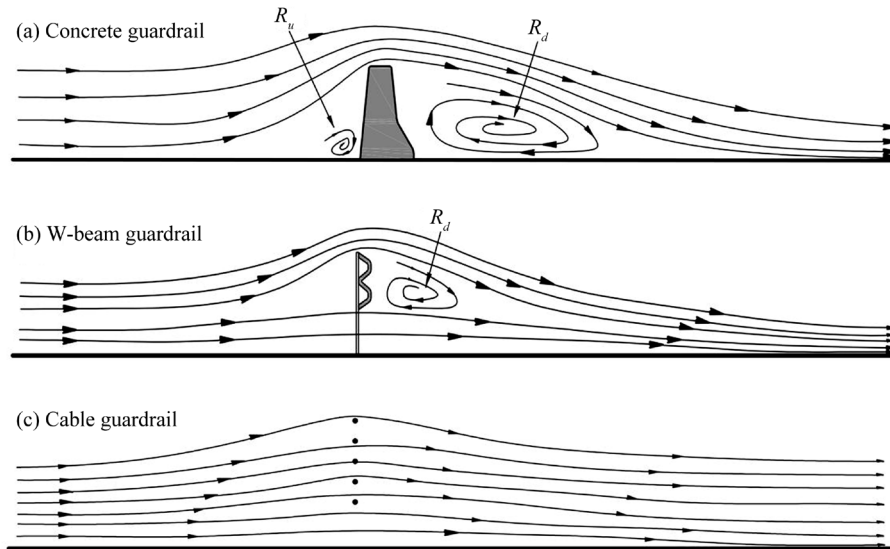


Fig. 6 Schematic diagram for streamline distribution around the guardrail. R_u is the clockwise vortex zone on the windward side, and R_d is the reversed flow region on the leeward side. (a), concrete guardrail; (b), W-beam guardrail; (c), cable guardrail.

3.2 Variation of wind velocity attenuation coefficient (WVAC)

Wind-blown sand movement is a sand conveying phenomenon close to the surface, and wind is the power source behind sand movement. The change of wind velocity near the surface determines the sand deposition distribution and sand transportation efficiency of the highway pavement on the leeward side of guardrail.

According to Equation 2, we calculated WVACs for the three types of guardrail at three heights (0.5H, 1.0H, and 3.0H), respectively, as shown in Figure 7. The vertical ordinate is WVAC, and the horizontal ordinate contains the positions of test points (positive values represent the windward side, negative values represent the leeward side, and 0 is the position of the guardrail). It can be seen that WVAC for the concrete and W-beam guardrails varied greatly between -0.230 and 1.000 , while the cable guardrail only ranged from -0.080 to 0.207 . As wind velocity increased, WVAC curves for the three types of guardrail did not change significantly overall, but the change trends varied greatly at different heights. At 0.5H and 1.0H, the rising and falling sections on the curves clearly changed, while the wind velocity on the leeward side decreased significantly, but at 3.0H, the curve changed smoothly with smaller fluctuation.

For the concrete guardrail, in the range of 1.0H–5.0H (shown by the red dotted line in the figure) and at 0.5H and 1.0H, WVAC varied smoothly between 0.859 and 1.000, indicating that the guardrail had a significant weakening effect on airflow at 1.0H height. Wind velocity attenuated sharply, and in the vortex zone, the creeping and saltating sand grains may deposit. In the interval from 0.0H to 10.0H on the leeward side, at a height of 3.0H, WVAC was less than 0.000, with a negative value appearing, suggesting that the airflow was in the acceleration zone. In the range of 5.0H–10.0H on the windward side, WVAC was between 0.000 and 0.140, and the

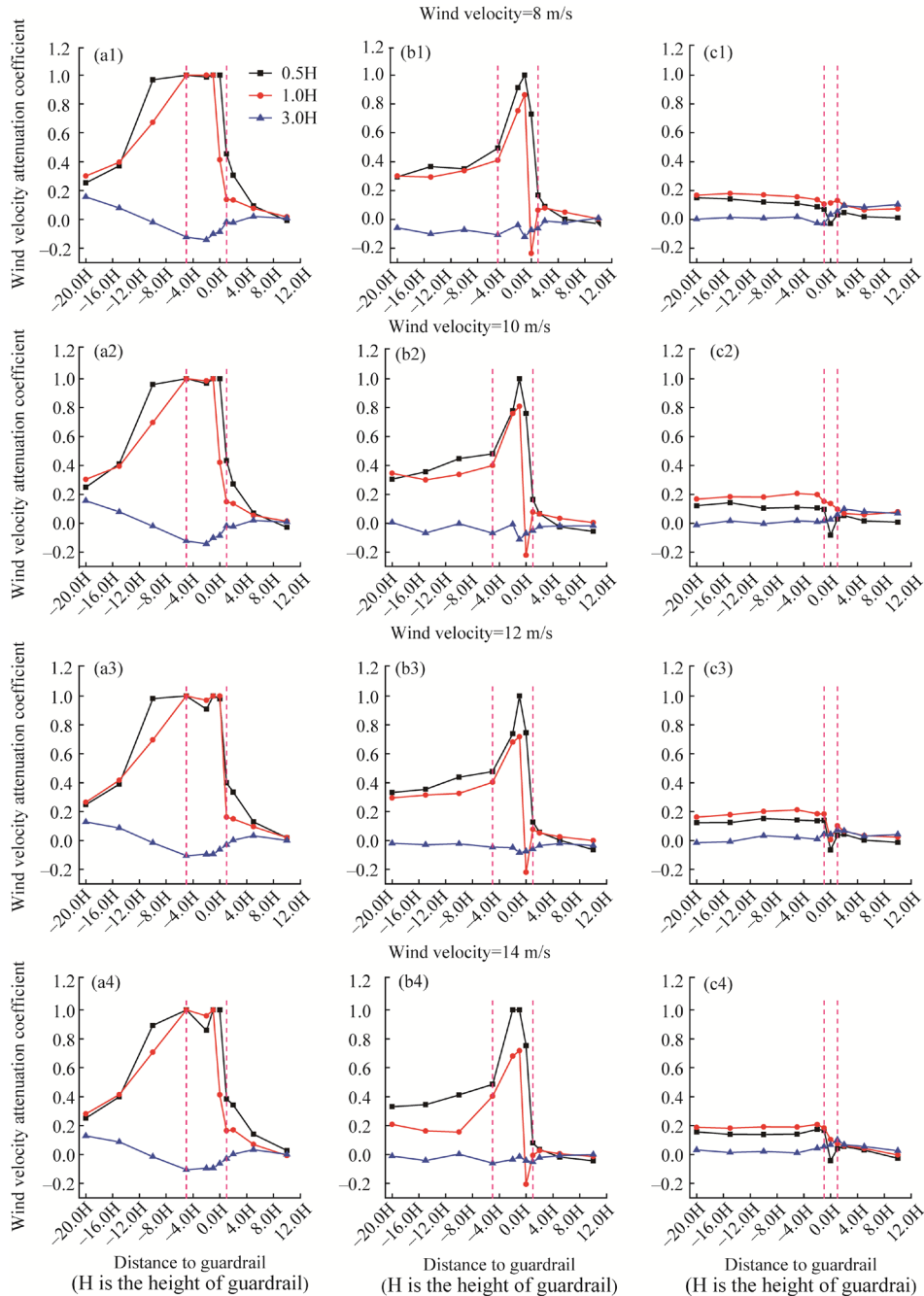


Fig. 7 Wind velocity attenuation coefficient (WVAC) of different types of guardrail under the wind velocities of 8, 10, 12, and 14 m/s. (a), concrete guardrail; (b), W-beam guardrail; (c), cable guardrail.

wind velocity was almost equal to the inflow wind velocity. WVAC in the range of $1.0H$ – $5.0H$ was between -0.028 and 0.430 . At heights of $0.5H$ and $1.0H$, WVAC suddenly increased from 0.430 to 1.000 in the range of $0.0H$ – $1.0H$, indicating that wind velocity rapidly decreased to 0.

In the range of $1.0H$ – $10.0H$ on the windward side, WVAC for the W-beam guardrail varied slightly, and wind velocity was consistent with the inflow velocity, while airflow was not affected by the guardrail. However, in the range of $1.0H$ – $2.0H$, WVAC below $1.0H$ rapidly increased above 0.600 , indicating that wind velocity on the windward and leeward sides of guardrail decreased significantly; while at $3.0H$, it decreased to a negative value and was in the acceleration

zone. WVAC decreased rapidly in the range of $2.0H$ – $5.0H$ and gradually stabilized from $5.0H$ to $20.0H$.

WVAC curve for the cable guardrail at different heights varied greatly in the range of $-1.0H$ – $1.0H$, with amplitude changes ranging from -0.100 to 0.200 . This result indicated that the incoming flow was affected by slight disturbance from the cable, and wind velocity changed slightly. WVACs at all heights varied smoothly from -0.050 to 0.200 in the range of $-5.0H$ – $-20.0H$ on the leeward side.

3.3 Sand transportation capacity of the highway pavement

To compare the influence of the three types of guardrail on sand transportation of desert highway pavement, we tested sand transportation quantity (STQ) and sand transportation efficiency (STE) for each guardrail using wind tunnel tests. Then, we summarized distribution characteristics of sand deposition on the highway pavement on the windward side of the guardrail.

3.3.1 STQ

STQ is one of the important indices to measure the degree of sand hazards in desert areas and the main basis for the design of sand prevention and control engineering. Desert highway pavement is smooth, and has a certain conveying capacity for sand grains in passing wind-blown sand. In the wind tunnel sand transportation tests, when there was no guardrail, the creeping and leaping sand grains in the height range of 20 cm above the pavement were carried away by the kinetic energy provided by the wind. The passing wind-blown sand moved smoothly to the highway downwind side, with no sand deposition on the highway surface. In this case, the sand sampler intercepted all sand grains transported within its height range. When guardrails were set, the cross-section of wind-blown sand decreased, the wind velocity decreased, the sand transportation capacity of wind-blown sand decreased, and some sand grains stagnated and were deposited on the road surface during transportation process. The sand sampler could only intercept part of the sand grains transported within its height range, i.e., STQ on the leeward side. The more the sand intercepted by the sand sampler, the greater the STQ of the guardrail, the better the sand transportation capacity of the highway pavement, and the less the sand that was deposited on the highway pavement.

Figure 8 shows STQ with and without guardrails at $5.0H$ on the leeward side at wind speeds of 8, 10, 12 and 14 m/s. Overall, in the height range of 0–10 cm, the order of STQ from more to less is as follows: empty field test is the most, followed by the cable guardrail, the W-beam guardrail ranked the third, and the concrete guardrail is the least. In the height range of 10–20 cm, there was no clear change in quantity. As height increased, STQ decreased gradually when the cable and W-beam guardrails were used, which indicated that sand transportation capacity decreased with heights. When the concrete guardrail was used, STQ was very low at all heights, less than $3 \text{ g}/(\text{cm}^2 \cdot \text{min})$, and there was no obvious change in quantity within the range of 0–10 cm. STQs increased slowly in the range of 10–20 cm. This result can be attributed the fact that the concrete guardrail was similar to a solid sand barrier. Sand grains were raised and suspended after wind-blown sand crossed the guardrail, resulting in the increased STQ above $1.0H$. With the increase of wind velocity, the STQs at various heights on the leeward side of guardrail gradually increased.

Table 1 shows the vertical distribution of STQ at $5.0H$ on the leeward sides of the three types of guardrail under the wind velocities of 8, 10, 12, and 14 m/s. The results showed that with the increase of wind velocity, STQ and total STQ (TSTQ) of the upper, middle and lower layers under the three types of guardrail increased, the percentage of relative STQ (RSTQ) of the lower layers (0–2 cm) close to the pavement decreased, RSTQ of the middle layers (3–10 cm) changed little, and RSTQ of the upper layers (11–20 cm) gradually increased. The result implied that the increase of wind velocity provided more kinetic energy to the wind-blown sand, and STQ of wind-blown sand increased, which increased the transportation height of sand grains and reduced the quantity of sand transported close to the highway pavement.

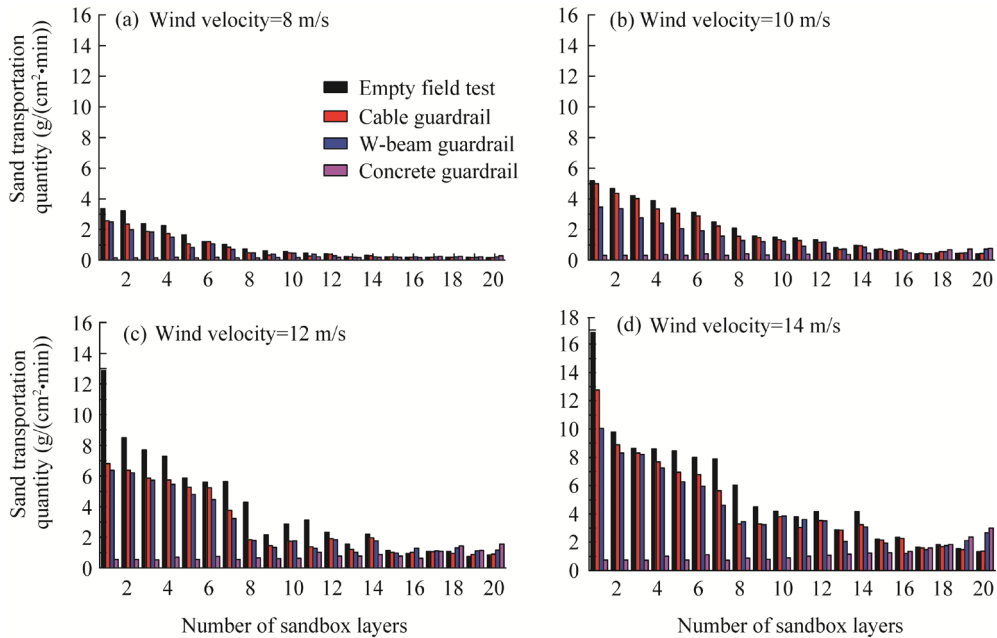


Fig. 8 Sand transportation quantity (STQ) of the highway pavement at 5.0H on the leeward side of guardrail under the wind velocities of 8 (a), 10 (b), 12 (c), and 14 m/s (d)

Table 1 Distribution of sand transportation quantity (STQ) on the highway pavement at 5.0H on the leeward side of guardrail under the wind velocities of 8, 10, 12, and 14 m/s

Type of guardrail	Layer	STQ (g/(cm ² ·min))	Wind velocity (m/s)			
			8	10	12	14
Concrete guardrail	All layer	Q_{0-20}	3.744	8.732	16.126	24.321
	Upper layer (11–20 cm)	Q_{11-20}	2.124	5.281	10.022	15.938
		RSTQ (%)	56.73	60.48	62.15	65.53
	Middle layer (3–10 cm)	Q_{3-10}	1.314	2.814	4.989	6.899
		RSTQ (%)	35.09	32.22	29.08	28.37
	Lower layer (0–2 cm)	Q_{0-2}	0.306	0.637	1.115	1.484
RSTQ (%)		8.17	7.29	6.91	6.10	
W-beam guardrail	All layer	Q_{0-20}	14.083	28.350	53.981	84.595
	Upper layer (11–20 cm)	Q_{11-20}	2.365	7.056	12.880	23.401
		RSTQ (%)	16.79	24.89	23.86	27.66
	Middle layer (3–10 cm)	Q_{3-10}	7.243	14.465	28.518	42.844
		RSTQ (%)	51.43	51.02	52.83	50.65
	Lower layer (0–2 cm)	Q_{0-2}	4.475	6.829	12.584	18.349
RSTQ (%)		31.78	24.09	23.310	21.69	
Cable guardrail	All layer	Q_{0-20}	15.192	36.687	56.341	90.633
	Upper layer (11–20 cm)	Q_{11-20}	2.263	7.434	12.289	23.236
		RSTQ (%)	14.90	20.26	21.81	25.64
	Middle layer (3–10 cm)	Q_{3-10}	8.016	19.896	30.877	45.754
		RSTQ (%)	52.76	54.23	54.80	50.48
	Lower layer (0–2 cm)	Q_{0-2}	4.913	9.356	13.177	21.644
RSTQ (%)		32.34	25.50	23.39	23.88	

Note: RSTQ, relative sand transportation quantity.

RSTQs with the W-beam and cable guardrails were concentrated in the middle and lower layers (0–10 cm). Under the wind velocities of 8, 10, 12, and 14 m/s, when a cable guardrail was used, RSTQs of the middle and lower layers were 85.10%, 79.73%, 78.19%, and 74.36%, respectively; when a W-beam guardrail was used, they were 83.21%, 75.11%, 76.14%, and 72.34%, respectively. The cable and W-beam guardrails are porous barriers, and sand grains in the height range of the guardrail were transported through the void. When the concrete guardrails were used, STQ was concentrated on the middle and upper layers (3–20 cm), where RSTQs were 91.82%, 92.7%, 91.23%, and 93.9%, respectively. Because the concrete guardrail is a solid sand barrier, sand grains of the middle and lower layers within the height of the guardrail were intercepted and deposited on the windward side of the guardrail, resulting in a reduction of STQ in the middle and lower layers of the highway pavement.

Figure 9 shows a comparison of STQ at different horizontal positions on the leeward side of the three types of guardrail under different wind velocities. It can be seen from Figure 9 that as wind velocity increased, STQ transported at each test point on the leeward side of the three types of guardrail gradually increased. In the range of 2.0H–5.0H, STQ on the highway pavement decreased significantly. STQ on the highway pavement behind the concrete guardrail decreased the most, from 60.60 to 3.74 g/(cm²·min), which indicated that the concrete guardrail might become a potential sand deposition zone. There was no significant change in STQ on the leeward side of the three types of guardrail in the range of 5.0H–20.0H. As wind velocity increased, STQ transported on the highway pavement behind the concrete guardrail did not increase significantly, and was between 3.37 and 23.71 g/(cm²·min), indicating that sand could still be deposited on the highway pavement at a higher wind velocity. STQ on the highway pavement behind the W-beam guardrail was between 15.38 and 94.67 g/(cm²·min), and behind the cable guardrail, it was between 15.16 and 89.27 g/(cm²·min). When the wind velocity was 8 m/s, STQ at each test point on the leeward side of the three types of guardrail was below 20 g/(cm²·min).

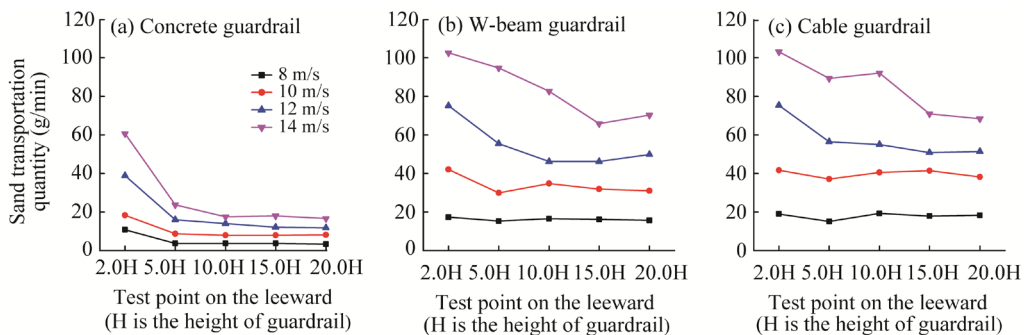


Fig. 9 Sand transportation quantity (STQ) of the highway pavement at different horizontal positions on the leeward side of guardrail. (a), concrete guardrail; (b), W-beam guardrail; (c), cable guardrail.

Figure 10 shows TSTQ on the leeward side of guardrail under four wind velocities. TSTQ on the highway pavement refers to the sum of quantities at five test points (2.0H, 5.0H, 10.0H, 15.0H, and 20.0H) on the leeward side of guardrail. It can be seen from Figure 10 that with the increase of wind velocity, TSTQ on the highway pavement on the leeward side of the three type of guardrail gradually increased, indicating that sand transportation capacity of wind-blown sand and STC of the highway pavement were enhanced. Thus, the sand grains were not easy to deposit. When the cable, W-beam and concrete guardrails were used and the wind velocity was 14 m/s, TSTQs were 423.53, 415.74, and 136.53 g/min, respectively. TSTQ on the highway pavement with the W-beam and cable guardrails was about three times greater than that of concrete guardrail, indicating that sand transportation capacity on the highway pavement with the cable and W-beam guardrails was better.

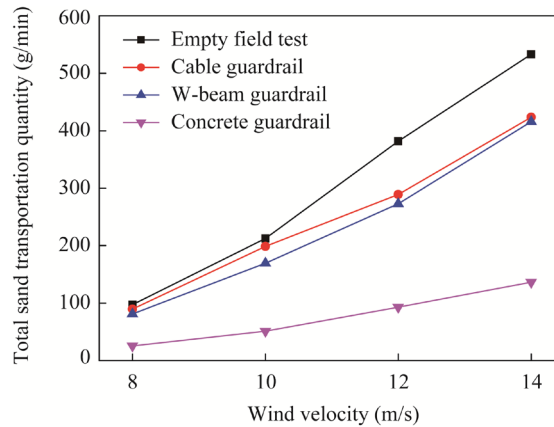


Fig. 10 Total sand transportation quantity (TSTQ) of the highway pavement on the leeward side of guardrail

3.3.2 STE

According to Equation 3, we calculated STE of desert highway pavement with the three types of guardrail under the wind velocities of 8, 10, 12, 14 m/s, respectively, as shown in Figure 11. It can be seen from Figure 11 that as wind velocity increased, there was no obvious fluctuation in STE curve under the three types of guardrail. From 2.0H to 20.0H on the leeward side of guardrail, STE with cable and W-beam guardrails decreased slowly overall. When a cable guardrail was used, STE of the highway pavement was the highest, ranging from 61.07% to 99.31%, with the best STC. When a W-beam guardrail was used, STE of the highway pavement was between 50.66% and 91.25%, slightly less than that of a cable guardrail. When a concrete guardrail was used, STE curve was more or less unchanged. STE was between 8.96% and 12.84%, with the worst STC.

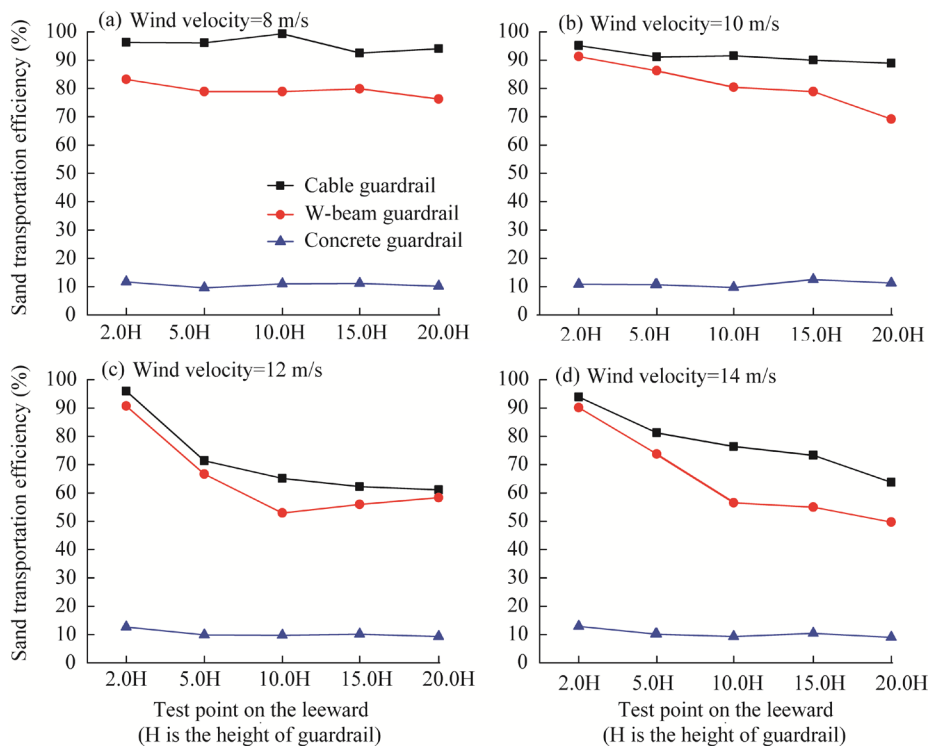


Fig. 11 Sand transportation efficiency (STE) of the highway pavement of different types of guardrail under the wind velocities of 8 (a), 10 (b), 12 (c), and 14 m/s (d)

3.4 Distribution of sand deposition on the highway pavement

Figure 12 shows sand deposition around the three types of guardrail under a wind velocity of 8 m/s. It can be seen that there were obvious differences in the sand deposition distribution around the three types of guardrail. Concrete guardrail was impervious to wind, and sand deposition was mainly distributed in the vortex zone of the corresponding flow field. The quantity of sand deposition on the windward side was significantly larger than on the leeward side, and deposition on the leeward side was mainly concentrated between $1.0H$ and $5.0H$. This result indicated that when the concrete guardrail was on the roadside of highway, it caused deposition on the shoulder and windward side of the highway pavement, and when it was located in the median separator, it caused sand deposition on both sides of the highway pavement. Deposition on the windward side of the W-beam guardrail formed strips with a small quantity of sand deposition behind $2.0H$ on the leeward side. The reason for this distribution was attributed to the fact that wind velocity decreased when airflow in the acceleration zone under the plate mixed with airflow in the upper vortex zone, so sand grains were deposited at a distance behind the guardrail. The airflow passing through the cable guardrail only increased the wind velocity variability, which was more conducive to the transport of sand grains. Therefore, there was no sand deposition on either the windward or leeward sides of the cable guardrail.

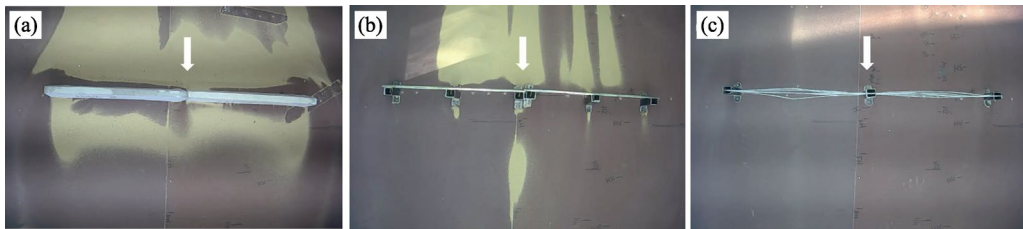


Fig. 12 Sand deposition around the guardrail. (a), concrete guardrail; (b), W-beam guardrail; (c), cable guardrail.

4 Discussion

To study the influence of different types of guardrails on sand transportation of desert highway pavement, the flow field, STQ, and STE around the guardrail were obtained through wind tunnel testing, and the vertical distribution characteristics of STQ and variability on the leeward side of guardrail were researched. Results showed that when a concrete guardrail was used, STE and TSTQ were the lowest, and the performance was the worst, easily causing sand deposition on the highway pavement. When a cable guardrail was used, the highest STE and TSTQ, and the best performance occurred on the highway pavement with no sand deposition. STC was slightly lower with a W-beam guardrail than with a cable guardrail. Therefore, from the perspective of effective sand transportation on the highway pavement, a cable guardrail should be used, followed by a W-beam guardrail, and a concrete guardrail was not suitable. However, cable guardrails are flexible, which may endanger driving safety in the opposite direction due to the large deformation caused by the low stiffness when a vehicle crashes. Therefore, it is inappropriate to arrange a cable guardrail at the median separator, and a W-beam guardrail would be more appropriate. Therefore, STQ and STE are important parameters to be considered in the design and optimization of desert highway guardrails.

Desert highway guardrails are traffic safety facilities, and sand barriers are used for wind-blown sand prevention along desert highways. When wind tunnel tests were conducted, the interaction between highway guardrails and wind-blown sand was similar to that of sand barriers, but different aspects were focused on. Sand barriers play the role of sand blocking, and reduce the ability of airflow to carry sand by reducing the kinetic energy of airflow around it, forcing sand grains to deposit nearby and avoiding sand deposition on the pavement. STC affected by the

guardrails was mainly concerned with, for example, reducing the resistance along the way during wind-blown sand movement, so that the passing wind-blown sand can smoothly pass through the pavement and move to the downwind side of the highway, producing effective sand transportation. The concrete guardrail was equivalent to pore-free solid sand barriers, while the W-beam and cable guardrails were equivalent to permeable solid sand barriers. There were two flow forms when airflows passed through the sand barrier: one was seepage through the sand barrier pores, and the other was detour flow through the sand barrier. Porosity will change the sand barrier air permeability (Tsukahara et al., 2012). With the change of wind velocity and porosity, the structure and partition of flow field around sand barriers will change (Bruno et al., 2018).

In this study, the three types of guardrail had different structures, wind resistance areas, wind ventilation areas, and porosity (Table 2). Concrete guardrail had no pore, a larger wake vortex zone, and more sand deposition. Studies have shown that when the sand barrier porosity greater than 20%–40%, the airflow is mainly controlled by flow at the pore, and the wake vortex zone disappears (Li and Sherman, 2015). The porosity of cable guardrail was 92.00%, and the flow field distribution characteristics were the same as the research results by Li and Sherman (2015). The porosity of the W-beam guardrail was 58.66%, and the wake zone behind the corrugated plate still had a small vortex zone, which was inconsistent with previous studies. We inferred that although the corrugated plate had higher porosity, from the structural trait, the upper part was an air-tight plate, and the lower part was fully air-permeable. The structure was similar to a lower wind deflector. A vortex zone occurred behind the plate before the air raised by the wind deflector converges with the air compressed through the plate lower outlet (Cheng et al., 2017; Han et al., 2017). Therefore, the wind ventilation and resistance areas of the guardrail are important factors affecting STC of the desert highway pavement.

Table 2 Wind ventilation area, wind resistance area, and porosity of the guardrail

Type of guardrail	Guardrail height H (cm)	Height of wind resistance H_1 (cm)	Height of wind ventilation H_2 (cm)	Wind resistance area per unit length A_1 (cm ² /cm)	Wind ventilation area per unit length A_2 (cm ² /cm)	Porosity (%)
Concrete guardrail	8.1	8.1	0.0	8.1	0.0	0.00
W-beam guardrail	7.5	3.1	4.4	3.1	4.4	58.66
Cable guardrail	11.3	0.9	10.4	0.9	10.4	92.00

Note: Porosity (%) is calculated by the following equation: $A_2/(A_1+A_2) \times 100\%$.

The subgrade of desert highway mainly includes embankment and cutting, with partial zero-fill subgrade, and half-fill and half-excavation subgrade (Fig. 1). In the design of highway engineering, guardrails must be set on both sides of an embankment and the filling side of a half-fill and half-excavation subgrade. Guardrails of desert highway not only need to ensure traffic safety, but also transport sand effectively on the highway pavement. Optimizing guardrail structure of desert highway pavement, improving STE and reducing the frequency and intensity of sand hazards will be the focus of future studies.

5 Conclusions

Wind tunnel tests were used to study the effects of concrete, W-beam and cable guardrails on sand transportation of desert highway pavement. Different types of guardrail had different effects on sand transportation, which were closely related to zoning characteristics of flow fields around the guardrail. Wind velocity isoline map of concrete guardrail showed three typical flow field zones. The interaction between the W-beam guardrail and wind-blown sand was similar to that of lower wind deflector. There was no obvious zoning in wind velocity isoline map around the cable guardrail, which had little disturbance effects on the airflow. WVAC showed that wind velocity on

the leeward side of the concrete and W-beam guardrails declined. Wind velocity attenuation amplitude on the leeward side of the W-beam guardrail was small, thus it was hard to deposit sand grains on the highway pavement. Wind velocity changed slightly on both sides of the cable guardrail. As wind velocity increased, STQ on the leeward side of the three types of guardrail gradually increased. Cable guardrail had the highest TSTQ and STE, concrete guardrail had the lowest, and W-beam guardrail was the medium. Sand grains were deposited contiguously on the windward and leeward sides of the concrete guardrail. When a W-beam guardrail was used, small amount of sand grains was deposited on the leeward side. There was no sand deposition on the windward and leeward sides of the cable guardrail. In conclusion, to realize effective sand transportation on the highway pavement and alleviate sand deposition hazards, the W-beam and cable guardrails should be used instead of the concrete guardrail in desert highways. Future research should focus on the influence of subgrade section form, topography, and the angle between dominant wind direction and subgrade. The synergistic effect of pavement sand transportation and sand control measures along the desert highway is also the research field.

Acknowledgements

This work was supported by the National Natural Science Foundation of China (52168065). The authors also thank the anonymous reviewers and the editor who helped to improve the quality of this paper.

References

- Bruno L, Horvat M, Raffaele L. 2018. Windblown sand along railway infrastructures: A review of challenges and mitigation measures. *Journal of Wind Engineering & Industrial Aerodynamics*, 177: 340–365.
- Chen B Y, Cheng J J, Xin L G, et al. 2019. Effectiveness of hole plate-type sand barriers in reducing aeolian sediment flux: Evaluation of effect of hole size. *Aeolian Research*, 38: 1–12.
- Cheng J J, Xue C X. 2014. The sand-damage-prevention engineering system for the railway in the desert region of the Qinghai-Tibet Plateau. *Journal of Wind Engineering & Industrial Aerodynamics*, 125: 30–37.
- Cheng J J, Lei J Q, Li S Y, et al. 2016a. Disturbance of the inclined inserting-type sand fence to wind-sand flow fields and its sand control characteristics. *Aeolian Research*, 21: 139–150.
- Cheng J J, Lei J Q, Li S Y, et al. 2016b. Effect of hanging-type sand fence on characteristics of wind-sand flow fields. *Wind and Structures*, 22(5): 555–571.
- Cheng J J, Zhi L Y, Xue C X, et al. 2017. Control law of lower air deflector for sand flow field along railway. *China Railway Science*, 38(6): 16–23. (in Chinese)
- Cheng J J, Ding B S, Gao L, et al. 2021. Numerical study on the bearing response trend of perforated sheet-type sand fences. *Aeolian Research*, 53: 100734, doi: 10.1016/j.aeolia.2021.100734.
- Ding B S, Cheng J J, Xia D T, et al. 2021. Fiber-Reinforced Sand-Fixing Board Based on the Concept of "Sand Control with Sand": Experimental Design, Testing, and Application. *Sustainability*, 13(18): 10229, doi: 10.3390/su131810229.
- Dong Z B, Chen G T, He X D, et al. 2004. Controlling blown sand along the highway crossing the Taklimakan Desert. *Journal of Arid Environments*, 57(3): 329–344.
- Han Y L, Gao Y, Meng Z J, et al. 2017. Effects of wind guide plates on wind velocity acceleration and dune leveling: a case study in Ulan Buh Desert, China. *Journal of Arid Land*, 9(5): 743–752.
- Han Z W, Wang T, Sun Q W, et al. 2003. Sand harm in Taklimakan Desert highway and sand control. *Journal of Geographical Sciences*, 13(1): 45–53.
- Jason M H, Venky N S, Gudmundur F U. 2005. The crash severity impacts of fixed roadside objects. *Journal of Safety Research*, 36(2): 139–147.
- Lei J Q, Li S Y, Fan D D, et al. 2008. Classification and regionalization of the forming environment of windblown sand disasters along the Tarim Desert Highway. *Chinese Science Bulletin*, 53(Suppl. 2): 1–7.
- Li B L, Sherman D J. 2015. Aerodynamics and morphodynamics of sand fences: A review. *Aeolian Research*, 17: 33–48.
- Li C J, Wang Y D, Lei J Q, et al. 2021. Damage by wind-blown sand and its control measures along the Taklimakan Desert Highway in China. *Journal of Arid Land*, 13(1): 98–106.
- Li S H, Li C, Yao D, et al. 2020. Wind tunnel experiments for dynamic modeling and analysis of motion trajectories of wind-blown sands. *European Physical Journal E*, 43(22): 1–10.

- Li S Y, Fan J L, Wang H F, et al. 2016. Causes and thoughts of comprehensive control of blown sand disaster at Qiaha Bridge of National Highway 315, in Cele County, Xinjiang, Northwest China. *Arid Land Geography*, 39(4): 754–760. (in Chinese)
- Owen P R, Gillette D. 1985. Wind tunnel constraint on saltation. In: *Proceedings of International Workshop on the Physics of Blown Sand*, Denmark: University of Aarhus, 253–269.
- Pan J S, Zhao H, Wang Y, et al. 2021. The influence of aeolian sand on the anti-Skid characteristics of Asphalt Pavement. *Materials*, 14(19): 5523, doi:10.3390/ma14195523.
- Shi L, Wang D Y, Cui K, et al. 2021. Comparative evaluation of concrete sand-control fences used for railway protection in strong wind areas. *Railway Engineering Science*, 29(2): 183–198.
- Tsukahara T, Sakamoto Y, Aoshima D, et al. 2012. Visualization and laser measurements on the flow field and sand movement on sand dunes with porous fences. *Experiments in Fluids*, 52(4): 877–890.
- Wang C, Li S Y, Li Z N, et al. 2020a. Effects of windblown sand damage on desert highway guardrails. *Natural Hazards*, 103: 283–298.
- Wang C, Li S Y, Lei J Q, et al. 2020b. Effect of the W-beam central guardrails on wind-blown sand deposition on desert expressways in sandy regions. *Journal of Arid Land*, 12(1): 154–165.
- Wang T, Qu J J, Niu Q H. 2020. Comparative study of the shelter efficacy of straw checkerboard barriers and rocky checkerboard barriers in a wind tunnel. *Aeolian Research*, 43: 1–11. <https://doi.org/10.1016/j.aeolia.2020.100575>.
- Wang Y G, Chen K M, Ci Y S, et al. 2011. Safety performance audit for roadside and median barriers using freeway crash records: Case study in Jiangxi, China. *Scientia Iranica*, 18(6): 1222–1230.
- White B R. 1996. Laboratory simulation of aeolian sand transport and physical modeling of flow around dunes. *Ann Arid Zone*, 35(3): 187–213.
- Xiao J H, Yao Z Y, Qu J J. 2015. Influence of Golmud-Lhasa section of Qinghai-Tibet Railway on blown sand transport. *Chinese Geographical Science*, 25(1): 39–50.